Available online at www.sciencedirect.com
SCIENCE DIRECT®
Journal of Power Sources 128 (2004) 145–151
JOURNAL OF POWER SOURCES
www.elsevier.com/locate/jpowsour

# Modeling the catalyst layer of a PEM fuel cell cathode using a dimensionless approach

K.T. Jeng*, C.P. Kuo, S.F. Lee

*Department of Mechanical and Automation Engineering, Dayeh University, Chang-Hwa 515-05, Taiwan*

Received 18 June 2003; received in revised form 17 September 2003; accepted 15 October 2003

**Abstract**

This paper presents the results of the modeling and analysis of the catalyst layer of a PEM fuel cell cathode. We nondimensionalized the governing equations and introduced three dimensionless parameters, $\pi_I$, $\pi_K$ and $\pi_D$, to simplify the description of the complicated phenomena occurring in the catalyst layer. The three dimensionless parameters indicate the resistance to oxygen reduction, the resistance to proton conduction, and the resistance to oxygen diffusion, respectively. The profiles of oxygen concentration, reaction rate, and current density in the catalyst layer were investigated in terms of $\pi_K$ and $\pi_D$. It was found that the dimensionless overpotential across the catalyst layer takes the form of $\hat{\eta}_{cat} = -\ln \pi_I - f(\pi_K, \pi_D)$. The functional relation of $f(\pi_K, \pi_D)$, which represents the mixture of ohmic overpotential and concentration overpotential, was then evaluated for various combinations of $\pi_K$ and $\pi_D$, and finally two correlation equations for $\hat{\eta}_{cat}$ were proposed. The plot of $f(\pi_K, \pi_D)$ and the proposed correlation equations are helpful for analysis, prediction and optimization of the performance of a PEM fuel cell.


*Keywords:* Fuel cell; Cathode; Catalyst layer; Modeling

## 1. Introduction

The cathodic overpotential, which constitutes the largest irreversible losses in the cell voltage, is influenced by several physical and operating parameters such as the cell current density, the active catalyst surface area, conductivities and thickness of the catalyst layer, the concentration and diffusion coefficient of oxygen, and so on. Mathematical models are a useful tool for analysis, prediction and optimization of the performance of the fuel cell cathode. Previous studies have offered many models for investigating the phenomena and overpotential occurring in the catalyst layer of a fuel cell electrode. The mathematical models devoted to the catalyst layer of a fuel cell electrode include the pseudo-homogeneous model [1–10], the single pore model [11], the thin film model [12], and the agglomerate model [4,12]. They incorporate different degrees of complexity and applicability. Among these models, the pseudo-homogeneous model is the one most often used, mainly because it is straightforward and its outcome compares well with experimental results. The pseudo-homogeneous model assumes that the catalyst layer has a uniform thickness and uniform distribution of its various components, i.e. the sizes of catalyst particles, ionomer, and gas pores are extremely small and are uniformly distributed throughout the catalyst layer.

The pseudo-homogeneous model has been adopted by the following studies in regard to the PEM fuel cell cathode. Bernardi and Verbruge [1,2] presented a complete model for a gas diffusion cathode bonded to a polymer electrolyte. They incorporated the electro-osmotic and pressure-driven water transport consonant of the PEM fuel cell to investigate the overpotential characteristics, water transport, and catalyst utilization. Springer et al. [3] developed a model considering, in detail, the voltage losses caused by interfacial kinetics at the Pt/ionomer interface, gas transport and proton conduction limitations, and gas transport limitations in the cathode backing. Broka and Ekdunge [4] studied the discrepancies in polarization curves given by the pseudo-homogeneous model and the agglomerate model under various values of oxygen permeability, conductivities and thickness of the catalyst layer. Marr and Li [7] used a mathematical model to study the performance of the cathode catalyst layer in a PEM fuel cell by including both electrochemical reaction, and mass transport processes.

* Corresponding author. Tel.: +886-4-851-1224; fax: +886-4-851-1224.
*E-mail address:* jeng@mail.dyu.edu.tw (K.T. Jeng).

0378-7753/$ – see front matter © 2003 Elsevier B.V. All rights reserved.
doi:10.1016/j.jpowsour.2003.10.004

The composition and performance optimization of catalyst platinum has also been investigated.

All previous studies on the pseudo-homogeneous model for the catalyst layer of a PEM fuel cell cathode have taken into account all the parameters influencing the performance of a fuel cell, and investigated their influences separately. Owing to the fact that the number of influential parameters is large, the analysis and optimization of a PEM fuel cell cathode turn out to be very complicated. However, the influential parameters can be organized into a lesser number of dimensionless groups, making the problem easier to deal with. In the present study we nondimensionalized the governing equations and boundary conditions, to reduce the description of the complicated phenomena occurring in the catalyst layer of a PEM fuel cell cathode to three dimensionless parameters. The cathodic overpotential was evaluated for various combinations of the dimensionless parameters, and then the relationship between the cathodic overpotential and the dimensionless parameters was obtained.

## 2. Model description

Fig. 1 presents a schematic of the cathode bonded to a proton exchange membrane in a PEM fuel cell. The system can be divided into three regions: a membrane region of solid polymer electrolyte (PEM), an active catalyst region (catalyst layer) that provides a catalytic site for the reduction of oxygen, and a diffusion region (gas diffusion layer) composed of highly porous and conductive material.

The gas diffusion layer is located adjacent to the air/$O_2$ flow channel and the current collector. Its open pores and electronically conductive material transport $O_2$ and electrons to the catalyst layer, respectively. The PEM is an electronic insulator, but an excellent conductor of protons. The protons produced at the anode go through the PEM to the catalyst layer of the cathode, where they react with electrons and $O_2$ to form $H_2O$. The catalyst layer is formed as a thin layer of proton conductive ionomer (e.g. Nafion®), and a carbon-supported catalyst (e.g. Pt/C). The ionomer portion

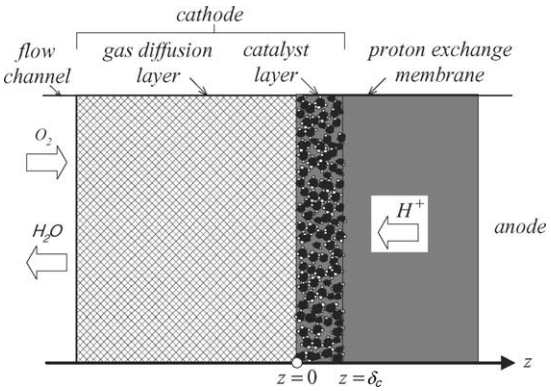


Fig. 1. Schematic of the cathode bonded to a proton exchange membrane in a PEM fuel cell.

of the catalyst layer forms the transport avenue for protons, and the matrix portion consisting of carbon and catalyst plays the role of electronic conductor. Studies on the microstructure of the catalyst layer have shown the existence of void space forming a network of gas channels that dominate the transport of $O_2$ to the active site [3,4,6].

In the present study we focus on the catalyst layer of the cathode, which is in the region of $0 < z < \delta_c$. In modeling this catalyst layer, the following assumptions have been adopted.

- The fuel cell is operating under a steady state.
- The catalyst layer is isothermal.
- The distribution of oxygen concentration, current density, and the overpotential in the catalyst layer is considered to be one dimensional.
- The oxygen permeation through the PEM is negligible.
- The catalyst layer can be regarded as a pseudo-homogeneous film, so that the active surface area of catalysts, void space and ionomer are uniformly distributed in it.
- The void space is sufficiently large so that the Knudsen diffusion is negligible [8,13]. Besides, the convective mass transfer of oxygen, driven by liquid water and water vapor, is unimportant compared to the bulk diffusion.
- The electronic conductivity of Pt/C is substantially greater than the protonic conductivity of ionomer [1,3,6,7].

The rate of the electrochemical reaction in the catalyst layer can be described using the Butler–Volmer rate expression. This is then simplified to give a Tafel-type equation in terms of the oxygen concentration as

$$\frac{\mathrm{d}i}{\mathrm{d}z} = A_\mathrm{v} i_0 \frac{C_{\mathrm{O}_2}}{C^*_{\mathrm{O}_2}} \exp\left(-\frac{\alpha_\mathrm{c} F\eta}{RT}\right) \tag{1}$$

In Eq. (1), $i$ is the local protonic current density, $A_\mathrm{v}$ the specific area of the active surface, $i_0$ the reference exchange current density, $C_{\mathrm{O}_2}$ the local oxygen concentration, $C^*_{\mathrm{O}_2}$ the reference oxygen concentration, which is associated with $i_0$, $\alpha_\mathrm{c}$ the cathodic transfer coefficient, and $\eta$ is the local cathodic overpotential.The local cathodic overpotential $\eta(z)$ is related to the potential difference of $\phi_\mathrm{s}(z)$ and $\phi_\mathrm{m}(z)$ by the equation:

$$\eta(z) = [\phi_\mathrm{s}(z) - \phi_\mathrm{m}(z)] - \phi_\mathrm{ref} \tag{2}$$

where $\phi_\mathrm{s}$ is the potential of the electronically conductive phase in the catalyst layer (i.e. the solid portion composed of carbon and catalyst particles), $\phi_\mathrm{m}$ the potential of the ionomer phase, and $\phi_\mathrm{ref}$ the reference potential difference. Both $\phi_\mathrm{s}$ and $\phi_\mathrm{m}$ increase in the positive $z$-direction, and equations of Ohm's law for each phase can be expressed as

$$\frac{\mathrm{d}\phi_\mathrm{s}}{\mathrm{d}z} = \frac{1}{K^\mathrm{eff}_\mathrm{s}}(I - i) \tag{3}$$

$$\frac{\mathrm{d}\phi_\mathrm{m}}{\mathrm{d}z} = \frac{1}{K^\mathrm{eff}_\mathrm{m}} i \tag{4}$$

where $I$ is the operating cell current density, $K_s^{eff}$ and $K_m^{eff}$ denote the effective conductivities of the solid portion and the ionomer phase, respectively. Therefore, the gradient of the overpotential in the catalyst layer is given by

$$\frac{d\eta}{dz} = \frac{1}{K_s^{eff}} I - \left( \frac{1}{K_m^{eff}} + \frac{1}{K_s^{eff}} \right) i \tag{5}$$

Because $K_s^{eff}$ is much greater than $K_m^{eff}$, Eq. (5) can be reduced to

$$\frac{d\eta}{dz} = -\frac{1}{K_m^{eff}} i \tag{6}$$

Note that the cathodic overpotential $\eta(z)$ and its first derivative $d\eta/dz$ are both negative. Therefore, $\eta(z)$ is a negative and monotonically decreasing function.

One can relate the oxygen concentration with the protonic current density $i$ in the catalyst layer by material balance. On the assumption that both convective mass transfer and Knudsen diffusion of oxygen are unimportant when compared to bulk diffusion, Fick's law completely describes the mass flux of oxygen in the catalyst layer. Moreover, as oxygen permeation through the PEM is negligible, the mass flux of oxygen crossing any location $z^*$ must be depleted in the region $z^* < z < \delta_c$. Hence the material balance for oxygen gives

$$\frac{dC_{O_2}}{dz} = -\frac{I - i}{4FD_{O_2}^{eff}} \tag{7}$$

where $D_{O_2}^{eff}$ is the effective diffusion coefficient of oxygen in the catalyst layer. Both $K_m^{eff}$ and $D_{O_2}^{eff}$ can be calculated from their bulk properties and volume fractions using the Bruggeman's correction [8,14,15], i.e. $K_m^{eff} = K_m \varepsilon_m^{3/2}$ and $D_{O_2}^{eff} = D_{O_2} \varepsilon^{3/2}$, where $\varepsilon_m$ is the volume fraction of ionomer, and $\varepsilon$ is the volume fraction of the open pores.

There are three dependent variables, $i$, $C_{O_2}$, and $\eta$, involved in three first-order differential equations, Eqs. (1), (6) and (7). Adopting the oxygen concentration at the gas diffusion layer/catalyst layer interface as the reference oxygen concentration, the corresponding boundary conditions are

$$i(\delta_c) = I \tag{8}$$

$$i(0) = 0 \tag{9}$$

$$C_{O_2}(0) = C_{O_2}^* \tag{10}$$

## 3. Solution technique

The governing equations and the corresponding boundary conditions together pose a boundary-value problem. This boundary-value problem can be reduced using the following relations: $\hat{z} = z/\delta_c$, $\hat{i} = i/I$, $\hat{C} = C_{O_2}/C_{O_2}^*$, $\hat{\eta} = \eta/b$, where $b = RT/\alpha_c F$ is the Tafel-slope. By introducing three dimensionless parameters, $\pi_I$, $\pi_K$, and $\pi_D$, the governing equations take the following form:

$$\frac{d\hat{i}}{d\hat{z}} = \frac{\hat{C}}{\pi_I} \exp(-\hat{\eta}) \tag{11}$$

$$\frac{d\hat{\eta}}{d\hat{z}} = -\pi_K \hat{i} \tag{12}$$

$$\frac{d\hat{C}}{d\hat{z}} = -\pi_D (1 - \hat{i}) \tag{13}$$

The corresponding boundary conditions become

$$\hat{i}(1) = 1 \tag{14}$$

$$\hat{i}(0) = 0 \tag{15}$$

$$\hat{C}(0) = 1 \tag{16}$$

The three $\pi$'s are meaningful dimensionless parameters in the characterization of the catalyst layer, and the solution of this problem is determined by the three $\pi$'s. Definitions and physical interpretations concerning the three $\pi$'s are as follows.

$\pi_I$ indicates a generalized resistance to oxygen reduction, which is expressed as the ratio of operating cell current density to exchange current density (based on geometric area), i.e.

$$\pi_I = \frac{I}{(A_v i_0)\delta_c} \sim \frac{\text{operating cell current density}}{\text{exchange current density}} \tag{17}$$

$\pi_K$ represents a normalized resistance to proton conduction, which is expressed as the ratio of the ohmic voltage drop across the catalyst layer to the Tafel-slope, i.e.

$$\pi_K = \frac{I\delta_c}{K_m^{eff} b} = \frac{I(\delta_c/K_m^{eff})}{b} \sim \frac{\text{ohmic voltage drop}}{\text{Tafel-slope}} \tag{18}$$

and $\pi_D$ is a normalized resistance to oxygen diffusion, which takes the form of the ratio of the oxygen consumption rate to the diffusive oxygen transport rate at a concentration gradient of $C_{O_2}^*/\delta_c$, i.e.

$$\pi_D = \frac{I\delta_c}{4FC_{O_2}^* D_{O_2}^{eff}} = \frac{I/4F}{D_{O_2}^{eff}(C_{O_2}^*/\delta_c)} \sim \frac{\text{oxygen consumption rate}}{\text{diffusive oxygen transport rate}} \tag{19}$$

In order to understand this problem better, we shall not solve Eqs. (11)–(13) directly. The coupled system of three first-order differential equations can be decoupled by differentiating Eq. (11) with respect to $\hat{z}$, and substituting $d\hat{\eta}/d\hat{z}$, $d\hat{C}/d\hat{z}$ into the so-obtained equation with the right-hand side of Eqs. (12) and (13), respectively. This then becomes

$$\frac{d^2\hat{i}}{d\hat{z}^2} = \left\{ \pi_D \frac{\hat{i} - 1}{\hat{C}} + \pi_K \hat{i} \right\} \frac{d\hat{i}}{d\hat{z}} \tag{20}$$

Eq. (20) can then be transformed into two first-order differential equations by the introduction of an additional variable $\hat{i}_p$, which stands for the dimensionless reaction rate. We now write

$$\frac{d\hat{i}}{d\hat{z}} = \hat{i}_p \tag{21}$$

$$\frac{d\hat{i}_p}{d\hat{z}} = \left\{ \pi_D \frac{\hat{i} - 1}{\hat{C}} + \pi_K \hat{i} \right\} \hat{i}_p \tag{22}$$

Eqs. (13), (21) and (22) represent the three dependent variables: $\hat{C}$, $\hat{i}$, and $\hat{i}_p$. Once their values at $\hat{z} = 0$ are designated, the nonlinear first-order initial-value problem can be solved to yield the $\hat{C}$, $\hat{i}$, and $\hat{i}_p$ profiles using numerical methods (e.g. the Runge–Kutta method). We already have the initial values of $\hat{i}(0) = 0$ and $\hat{C}(0) = 1$ from Eqs. (15) and (16). However, the value of $\hat{i}_p(0)$ must be chosen to ensure that the solution profiles satisfy Eq. (14). Consequently this results in a shooting problem that can be resolved by the appropriate shooting technique [16]. After obtaining the solutions to the initial-value problem, the profiles of $\hat{C}$ and $\hat{i}_p$ are then substituted into Eq. (11) to yield the spatial variation of $\hat{\eta}$.

## 4. Results and discussion

It is necessary to remark the facts that the dimensionless parameter $\pi_I$ has been eliminated through the derivation of Eq. (20), which was then transformed into Eqs. (21) and (22), and $\pi_I$ is not involved in Eq. (13). Thus, the spatial variation of the dimensionless reaction rate $\hat{i}_p$, protonic current density $\hat{i}$, and oxygen concentration $\hat{C}$, obtained by solving Eqs. (13), (21) and (22), is independent of $\pi_I$. Their solution profiles are determined only by both $\pi_K$ and $\pi_D$. This interesting phenomenon signifies that, for a fixed set

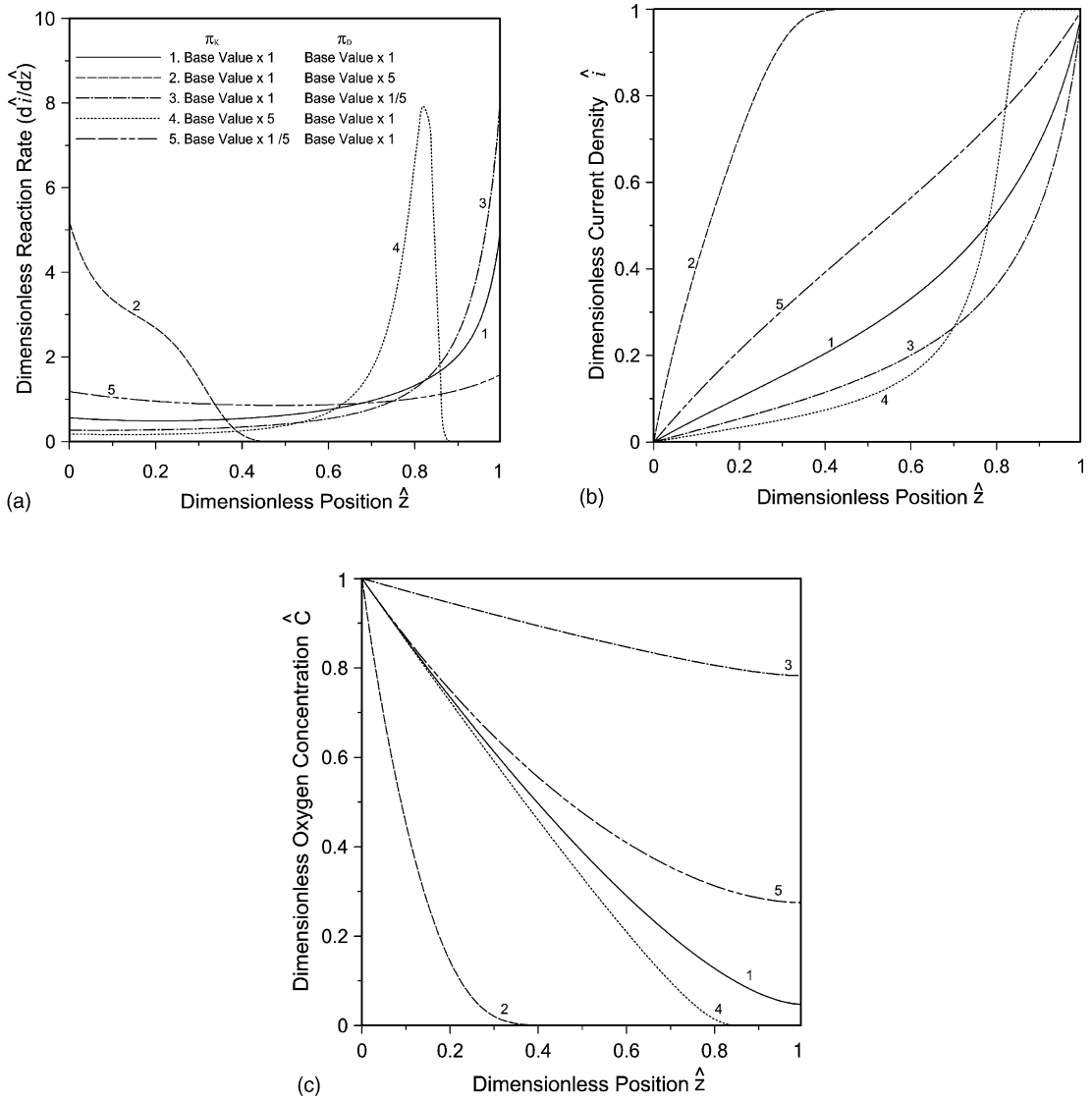


Fig. 2. Influence of $\pi_K$ and $\pi_D$ on the dimensionless spatial variation of (a) reaction rate, (b) current density, and (c) oxygen concentration.

Table 1
Electrode properties and physical parameters for base-case conditions

| Electrode property/physical parameter | Values |
|---|---|
| Cell temperature, $T$ (K) | 353 |
| Cell current density, $I$ (A/cm$^2$) | 0.5 |
| Cathodic transfer coefficient, $\alpha_c$ | 2.0 |
| Reference exchange current density times area, $A_v i_o$ (A/cm$^3$) | $5 \times 10^{-4}$ [1] |
| Catalyst layer thickness, $\delta_c$ (cm) | 0.001 |
| Reference oxygen concentration, $C^*_{O_2}$ (mol/cm$^3$) | $4.62 \times 10^{-6}$ [1] |
| Effective protonic conductivity in catalyst layer, $K_m^{eff}$ (S/cm) | 0.002 [3] |
| Effective diffusion coefficient of oxygen in catalyst layer, $D^{eff}_{O_2}$ (cm$^2$/s) | $2\times10^{-4}$ [3] |

of $\pi_K$ and $\pi_D$ values, decreasing the value of $\pi_I$ (e.g. the method of increasing the catalyst density) will not alter the profiles of reaction rate $\hat{i}_p$, protonic current density $\hat{i}$, and oxygen concentration $\hat{C}$, but $|\hat{\eta}|$ will be decreased according to Eq. (11). Fig. 2 shows the influence of $\pi_K$ and $\pi_D$ on the spatial variation of $\hat{i}_p$, $\hat{i}$, and $\hat{C}$ in the catalyst layer. The base values of $\pi_I$, $\pi_K$ and $\pi_D$ are $1 \times 10^6$, 16.43, and 1.402, respectively, and they are evaluated from the base-case conditions given in Table 1.

It can be seen that the oxygen concentration profile drops rapidly (see Fig. 2c) as the value of $\pi_D$ is increased to five times its base value. A large $\pi_D$ indicates low oxygen permeability, so the oxygen concentration is extremely low in the right portion of the catalyst layer. Accordingly, the distribution of the reaction rate (see Fig. 2a) shifts to the left, and no oxygen reduction occurs in the right portion. As the value of $\pi_D$ decreases to one-fifth of the base value the oxygen will penetrate the catalyst layer more easily, thus the oxygen concentration profile becomes more uniform and the distribution of the reaction rate shifts to the right.

In contrast to the effect of changing the value of $\pi_D$, increasing the value of $\pi_K$ to five times its base value, the reaction rate in the left portion decreases noticeably because the resistance to proton conduction is increased. Instead of shifting to the right-most boundary, the reaction rate peaks around $z = 0.8$. This is due to the fact that the oxygen diffusion is not high enough to provide a good penetration through the catalyst layer, so most of the oxygen is consumed somewhere off the catalyst layer/PEM interface. If we reduce the value of $\pi_K$ to one-fifth of the base value, the resistance to proton conduction is lowered, hence, the protons are transported to the left more easily, and the distribution of reaction rate tends to level off.

Inserting the solution profiles of $\hat{C}$ and $\hat{i}_p$ into Eq. (11) the spatial variation of the dimensionless overpotential $\hat{\eta}$ is readily obtained. Fig. 3 gives the solution profiles for the base value of $\pi_I$ associated with the same five combinations of $\pi_K$ and $\pi_D$ used in Fig. 2. As pointed out above, when referring to Eq. (6), the solution profile of $\hat{\eta}$ is a negative, monotonically decreasing function. Higher values of $\pi_K$ and $\pi_D$ indicate greater hindrance to the transport of proton and

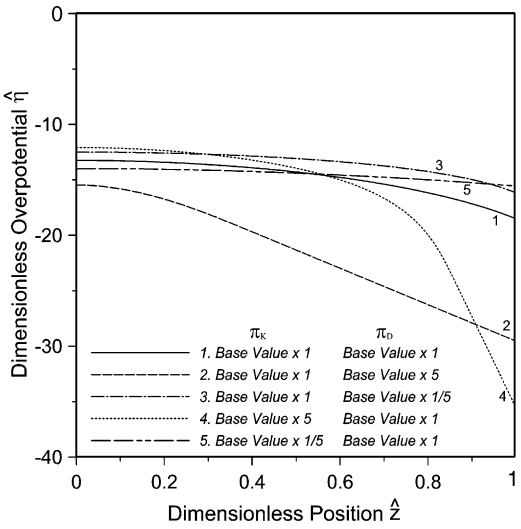


Fig. 3. Spatial variation of dimensionless cathodic overpotential throughout the catalyst layer for the same combinations of $\pi_K$ and $\pi_D$ used in Fig. 2.

oxygen, hence more voltage losses occur across the catalyst layer. As can be seen, for a given value of $\pi_I$, increasing the values of $\pi_K$ and $\pi_D$ causes a greater overpotential across the catalyst layer, and vice versa.

The main purpose of this study is to investigate the influence of $\pi_I$, $\pi_K$ and $\pi_D$ on the dimensionless overpotential associated with the whole cathodic catalyst layer, which we designate as $\hat{\eta}_{cat}$. As depicted in Fig. 3, the local overpotential varies throughout the catalyst layer. In this study we take $\hat{\eta}_{cat} = \hat{\eta}(1)$ because $\hat{\eta}(1)$ is equal to the experimentally measured dimensionless cathodic overpotential [3,6]. From Eq. (11) and the foregoing analysis, it is perceived that the dimensionless overpotential associated with the cathodic catalyst layer, $\hat{\eta}_{cat}$, is governed by $\pi_I$, $\hat{C}(1)$, and $\hat{i}_p(1)$. The latter two are in turn governed by $\pi_K$ and $\pi_D$. We deduce that the relationship among $\hat{\eta}_{cat}$, $\pi_I$, $\pi_K$ and $\pi_D$ can be expressed as

$$\hat{\eta}_{cat} = -\ln \pi_I - f(\pi_K, \pi_D) \tag{23}$$

The influence of $\pi_I$ on $\hat{\eta}_{cat}$ can be decoupled from $\pi_K$, $\pi_D$ and takes a logarithmic form, whereas the influence of both $\pi_K$ and $\pi_D$ are coupled together. The first term on the right-hand side of Eq. (23) represents the activation overpotential, and the second term stands for the mixture of ohmic overpotential and concentration overpotential. The unknown function $f(\pi_K, \pi_D)$ can be determined by evaluating $\hat{\eta}_{cat}$ for a given value of $\pi_I$ associated with various combinations of $\pi_K$ and $\pi_D$. Fig. 4 shows the curves of $f(\pi_K, \pi_D)$ for some constant values of $\pi_D$ with respect to the variation of $\pi_K$. This figure presents the curves of $f(\pi_K, \pi_D)$ up to a function value of 60, which is equivalent to 0.913 V in the mixture of ohmic overpotential and concentration overpotential (base-case values, $\alpha_c = 2.0$, and $T = 353$ K, are applied). This range is wide enough to cover the entire operating conditions of a PEM fuel cell.

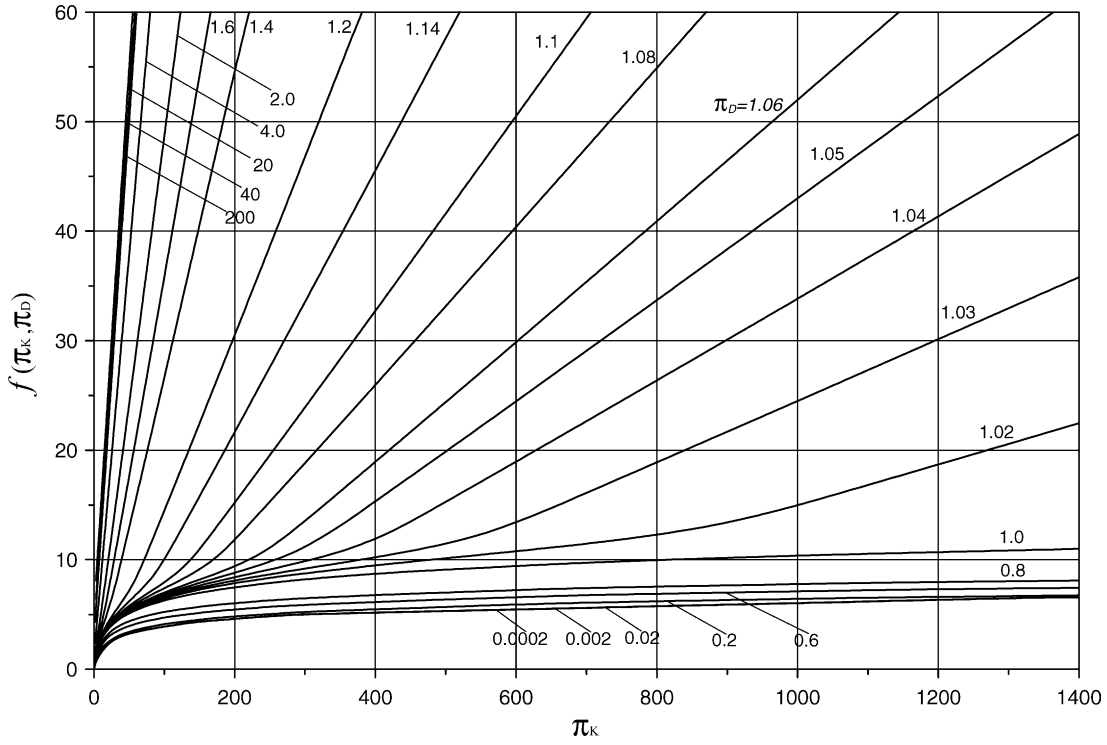


Fig. 4. Mixture of ohmic and concentration overpotential as a function of $\pi_K$ and $\pi_D$.

As depicted in Fig. 4, the function value of $f(\pi_K, \pi_D)$ approaches zero as both $\pi_K$ and $\pi_D$ approach zero. Thus, Eq. (23) reduces to $\hat{\eta}_{cat} = -\ln \pi_I$ under any one of the following conditions: (i) the thickness of the catalyst layer is extremely thin, (ii) the current density is extremely low, and (iii) both the effective conductivity $K_m^{eff}$ and the effective diffusion coefficient $D_{O_2}^{eff}$ are extremely high.

It can be seen from Fig. 4 that $f(\pi_K, \pi_D)$ is an increasing function of $\pi_K$ and $\pi_D$. In Fig. 4, one can see that the curves for $\pi_D > 20$ coincide with that of $\pi_D = 20$. The reason for this lies in the limitation of resistance to oxygen diffusion. With the value of $\pi_D$ approaching 20, the oxygen diffusion becomes very slow, and the oxygen concentration profile drops abruptly to zero. Thus, the reduction of oxygen takes place only within an extremely thin layer, or is even restricted to the left-most boundary. When this happens, increasing the value of $\pi_D$ will not further increase the cathodic overpotential. On the other hand, the curves for $\pi_D < 0.02$ coincide with that of $\pi_D = 0.02$. This indicates that, with the resistance to oxygen diffusion already being very small, $\pi_K$ is the only controlling factor of $f(\pi_K, \pi_D)$. Hence, furthering the diffusion capability of oxygen will not lower the cathodic overpotential.

An empirical correlation can be developed for the functional form of $f(\pi_K, \pi_D)$ utilizing the curves shown in Fig. 4. With $\pi_D$ being fixed and greater than 1.2, a linear relationship between the function value and $\pi_K$ is observed. Also, for $\pi_D$ being smaller than 0.8, a semi-logarithmic relationship is found. The coefficients of correlation can be obtained by regression analysis, and the following correlation equations are suggested:

$$f(\pi_K, \pi_D) = \left(\frac{1 - \pi_D}{-0.1216 - 0.9635\pi_D}\right)\pi_K, \quad \pi_D \geq 1.2 \tag{24}$$

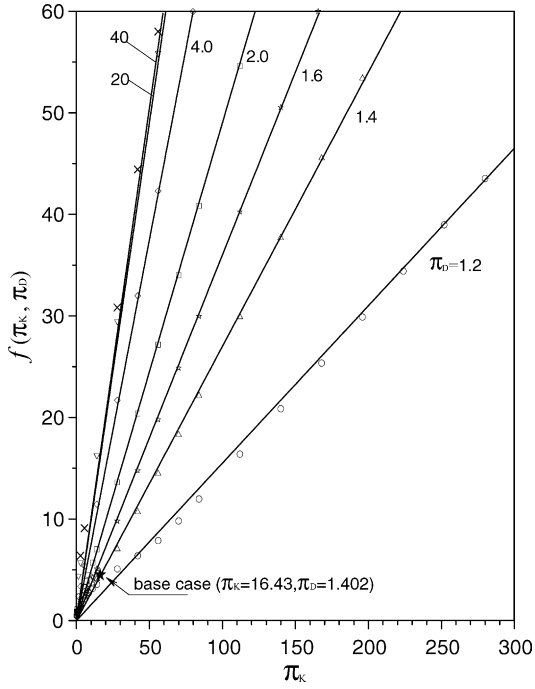


Fig. 5. Fit of Eq. (24) to the calculated function values for $\pi_D \geq 1.2$.

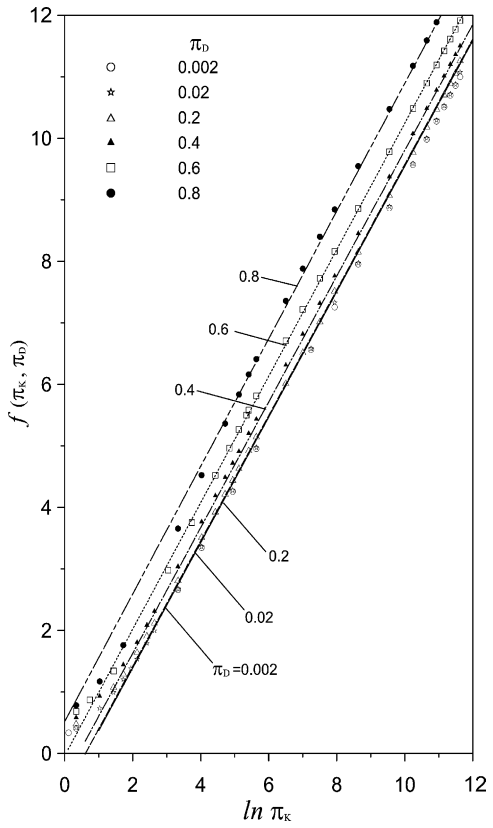


Fig. 6. Fit of Eq. (25) to the calculated function values for $\pi_D \leq 0.8$.

and

$$f(\pi_K, \pi_D) = (-0.65 - 0.3\pi_D + 2.2{\pi_D}^2) + 1.025 \ln \pi_K, \quad \pi_D \leq 0.8 \qquad (25)$$

Figs. 5 and 6 respectively show the fit of the correlation equations to the calculated function values. As shown in both these figures, the two correlation equations are in good agreement with the calculated function values. The maximal error in correlation, which occurs in the low $\pi_K$ region, is estimated to be 2.1 for Eq. (24), and 0.65 for Eq. (25). They are respectively equivalent to 0.032 and 0.01 V in overpotential when the base-case values of cell temperature $T$ and transfer coefficient $\alpha_c$ are applied.

## 5. Conclusions

A mathematical model for the catalyst layer of a PEM fuel cell cathode has been developed, the formulated equations were nondimensionalized, and were then reduced to a system of dimensionless differential equations associated with three dimensionless parameters, $\pi_I$, $\pi_K$ and $\pi_D$. Here, $\pi_I$ represents the resistance to oxygen reduction, $\pi_K$ the resistance to proton conduction, and $\pi_D$ the resistance to oxygen diffusion, hence they are responsible for the activation overpotential, ohmic overpotential, and concentration overpotential, respectively. This approach has simplified the presentation of complicated results relevant to the catalyst layer, and offered a useful tool for the investigation into the PEM fuel cell cathode.

The profiles of oxygen concentration, reaction rate, and current density are governed only by $\pi_K$ and $\pi_D$. They influence the cathodic overpotential through the spatial variations of reaction rate, and oxygen concentration. The influence of $\pi_I$ on $\hat{\eta}_{cat}$ can be decoupled from $\pi_K$, $\pi_D$ and takes a logarithmic form, whereas the influence of both $\pi_K$ and $\pi_D$ are coupled together. The dependence of the mixture of ohmic overpotential and concentration overpotential on $\pi_K$ and $\pi_D$ was depicted in Fig. 4, which can be conveniently referred to when assessing the performance of a PEM fuel cell.

Further more, an empirical correlation was developed using the results presented in Fig. 4. This has yielded the following two correlation equations:

$$\hat{\eta}_{cat} = -\ln \pi_I + \left(\frac{1 - \pi_D}{0.1216 + 0.9635\pi_D}\right)\pi_K, \quad \pi_D \geq 1.2 \qquad (26)$$

$$\hat{\eta}_{cat} = -\ln \pi_I + (0.65 + 0.3\pi_D - 2.2{\pi_D}^2) - 1.025 \ln \pi_K, \quad \pi_D \leq 0.8 \qquad (27)$$

This correlation is considered to be helpful for the analysis, prediction and optimization of the performance of a PEM fuel cell.

## References

[1] D.M. Bernardi, M.W. Verbrugge, AIChE J. 37 (8) (1991) 1151.
[2] D.M. Bernardi, M.W. Verbrugge, J. Electrochem. Soc. 139 (9) (1992) 2477.
[3] T.E. Springer, M.S. Wilson, S. Gottesfeld, J. Electrochem. Soc. 140 (12) (1993) 3513.
[4] K. Broka, P. Ekdunge, J. Appl. Electrochem. 27 (1997) 281.
[5] K. Scott, W. Taama, J. Cruickshank, J. Power Sour. 65 (1997) 159.
[6] M. Eikerling, A.A. Kornyshev, J. Electroanal. Chem. 453 (1998) 89.
[7] C. Marr, X. Li, J. Power Sour. 77 (1999) 17.
[8] J.J. Baschuk, X. Li, J. Power Sour. 86 (2000) 181.
[9] H. Dohle, J. Divisek, R. Jung, J. Power Sour. 86 (2000) 469.
[10] K.T. Jeng, C.W. Chen, J. Power Sour. 112 (2002) 367.
[11] S. Srinivasan, H.D. Hurwitz, O.M. Bockris, J. Chem. Phys. 46 (8) (1967) 3108.
[12] Y. Bultel, P. Ozil, R. Durand, Electrochim. Acta 43 (9) (1998) 1077.
[13] C.N. Satterfield, Mass Transfer in Heterogeneous Catalysis, MIT Press, Cambridge, 1970.
[14] C.W. Tobias, Advances in Electrochemistry and Electrochemical Engineering, Wiley, New York, 1962, p. 19.
[15] C. Marr, X. Li, ARI 50 (1998) 190.
[16] J.D. Faires, R. Burden, Numerical Methods, Brooks/Cole, Pacific Grove, CA, 1998, p. 439.